NASA/TM—2007–215075

Study of Radiographic Linear Indications and Subsequent Microstructural Features in Gas Tungsten Arc Welds of Inconel 718

J.L. Walley
Universities Space Research Association, Huntsville, Alabama

A.C. Nunes
Marshall Space Flight Center, Marshall Space Flight Center, Alabama

J.L. Clounch
Jacobs ESTS Group, Huntsville, Alabama

C.K. Russell
Marshall Space Flight Center, Marshall Space Flight Center, Alabama

September 2007

The NASA STI Program…in Profile

Since its founding, NASA has been dedicated to the advancement of aeronautics and space science. The NASA Scientific and Technical Information (STI) Program Office plays a key part in helping NASA maintain this important role.

The NASA STI program operates under the auspices of the Agency Chief Information Officer. It collects, organizes, provides for archiving, and disseminates NASA's STI. The NASA STI program provides access to the NASA Aeronautics and Space Database and its public interface, the NASA Technical Report Server, thus providing one of the largest collections of aeronautical and space science STI in the world. Results are published in both non-NASA channels and by NASA in the NASA STI Report Series, which includes the following report types:

- TECHNICAL PUBLICATION. Reports of completed research or a major significant phase of research that present the results of NASA programs and include extensive data or theoretical analysis. Includes compilations of significant scientific and technical data and information deemed to be of continuing reference value. NASA's counterpart of peer-reviewed formal professional papers but has less stringent limitations on manuscript length and extent of graphic presentations.

- TECHNICAL MEMORANDUM. Scientific and technical findings that are preliminary or of specialized interest, e.g., quick release reports, working papers, and bibliographies that contain minimal annotation. Does not contain extensive analysis.

- CONTRACTOR REPORT. Scientific and technical findings by NASA-sponsored contractors and grantees.

- CONFERENCE PUBLICATION. Collected papers from scientific and technical conferences, symposia, seminars, or other meetings sponsored or cosponsored by NASA.

- SPECIAL PUBLICATION. Scientific, technical, or historical information from NASA programs, projects, and missions, often concerned with subjects having substantial public interest.

- TECHNICAL TRANSLATION. English-language translations of foreign scientific and technical material pertinent to NASA's mission.

Specialized services also include creating custom thesauri, building customized databases, and organizing and publishing research results.

For more information about the NASA STI program, see the following:

- Access the NASA STI program home page at <http://www.sti.nasa.gov>

- E-mail your question via the Internet to <help@sti.nasa.gov>

- Fax your question to the NASA STI Help Desk at 301– 621–0134

- Phone the NASA STI Help Desk at 301– 621–0390

- Write to:
  NASA STI Help Desk
  NASA Center for AeroSpace Information
  7115 Standard Drive
  Hanover, MD 21076–1320

Study of Radiographic Linear Indications and Subsequent Microstructural Features in Gas Tungsten Arc Welds of Inconel 718

J.L. Walley
Universities Space Research Association, Huntsville, Alabama

A.C. Nunes
Marshall Space Flight Center, Marshall Space Flight Center, Alabama

J.L. Clounch
Jacobs ESTS Group, Huntsville, Alabama

C.K. Russell
Marshall Space Flight Center, Marshall Space Flight Center, Alabama

Acknowledgments

TRADEMARKS

Available from:

NASA Center for AeroSpace Information
7115 Standard Drive
Hanover, MD 21076–1320
301–621–0390

This report is also available in electronic form at
<https://www2.sti.nasa.gov>

TABLE OF CONTENTS

LIST OF FIGURES

LIST OF TABLES

LIST OF ACRONYMS AND SYMBOLS

Al	aluminum
AMET	Automated Manufacturing Engineering Technologies
C	carbon
Cr	chromium
Cu	copper
Fe	iron
GTAW	gas tungsten arc welding
Mo	molybdenum
Nb	niobium
NDE	nondestructive evaluation
Ni	nickel
Ti	titanium
UTS	ultimate tensile strength
VPPA	variable polarity plasma arc

NOMENCLATURE

a	parameter
h	coordinate of reciprocal lattice point hkl
I	intensity
L	effective distance from the diffracting body
w	width
x	distance traveled
ϕ	angle of reflected beam
λ	wavelength
θ	angle of reciprocal lattice
μ	absorption coefficient

TECHNICAL MEMORANDUM

STUDY OF RADIOGRAPHIC LINEAR INDICATIONS AND SUBSEQUENT MICROSTRUCTURAL FEATURES IN GAS TUNGSTEN ARC WELDS OF INCONEL 718

1. INTRODUCTION

Assessment of the integrity of a weld is a complicated, nondestructive evaluation (NDE) problem that can be challenging to even the most trained specialist. Many of today's aerospace materials, such as Inconel® 718 (registered trade name of Inco Alloys International, Inc.) (AMS 5596J) do not have a set of reference guides for the specialist to make comparisons. This makes identifying hazardous defect indications an art form, subject to personal acuity, experience, and interpretations. This study was conducted to produce linear radiographic indications from 0.05-in-thick Inconel 718 butt welds and to identify the microstructural elements causing each of the indications.

The focus of this study was to provide a procedure for differentiating different types of indications like enigma, or 'ghost,' indications from indications produced by potentially hazardous defects. An enigma indication can be misinterpreted as deriving from real weld defects such as lack of fusion or penetration, but are caused by some other structural characteristic that may or may not be detrimental to the integrity of the weld joint. Enigmas have been found in variable polarity plasma arc (VPPA) welds of aluminum alloys due to elemental segregation of copper (Cu) during solidification. The purpose of this study was to further the understanding of the formation of enigmas in Inconel 718 weld radiographs[1] so that more accurate interpretations can be accomplished during NDE.

Initial information has been provided on the material under investigation, a definition of a radiographic enigma, and a highlight of some of its common structural causes. The experimental procedures used in this investigation to produce nominal welds, enigma indications, and defect indications have been explained. Radiographic and microscopic observations have also been explained and compared, as well as eddy current and penetrant observations on select weld joints. Findings have been summarized and recommendations made for distinguishing radiographic enigma indications from indications produced by defects.

2. MATERIAL BACKGROUND

Inconel 718 is a niobium (Nb)-strengthened nickel (Ni)-iron (Fe) superalloy. Nominal composition is given in table 1. The Nb content acts to strengthen the alloy through precipitates of γ'' particles of the Ni_3Nb ordered, face centered cubic phase. These precipitates limit the solubility of the γ' phase, $Ni_3(Ti, Al)$, also used to harden Ni-Fe superalloys. Both of these precipitates give the Ni-Fe superalloy its higher strength at elevated temperatures; this is due to resistance to dislocation cutting through the precipitates. The added benefit of γ'', which forms around the γ' particles, is its slow transformation rate. This greatly enhances the weldability of the superalloy over others because it does not instantly induce hardening and consequent postweld cracking.[2–4] The overall complexity of this structure causes a tendency toward dendrite formation during welding.[5,6]

Table 1. Inconel 718 nominal alloy composition (wt%).[4]

Ni	Cr	Mo	Nb	Ti	Al	Fe	C	Cu
53	19	3	5.1	0.9	0.5	18.5	0.08	0.15

3. COMMON RADIOGRAPHIC INDICATIONS

Determining a method for discerning different defects by means of their radiographic linear indications as observed in gas tungsten arc welding (GTAW) welds was the intention of this study. Each defect is associated with a different type of indication. Examples of defects and their common indications as presented in the *Nondestructive Testing Handbook* are listed below:[7]

- Incomplete (or lack of) penetration is an absence of fusion at the weld root. It may be caused by an insufficiently hot root pass. It is indicated by a broad line along the weld. The line may be located along the weld centerline or be offset depending upon the alignment of the weld bead with the weld seam. The width of the indication is a function of the amount of incomplete penetration.

- Incomplete (or lack of) fusion is an absence of fusion between a weld bead and adjacent metal. It may be caused by improper welding technique. The unfused gap tends to be narrow and to produce a sharp, dark line indication when lined up along the x-ray beam.

- Tungsten inclusions (from a GTAW electrode) are usually denser than the weld metal and appear as light spots on a radiograph.

- Shrinkage comprises irregular cavities or distributions of irregular cavities. It occurs when a solidifying volume of molten metal is sealed off from a source of replenishing molten metal so that cavities open up between solidifying dendrites. Indications are dark and may range from shadowed areas for a distribution of microshrinkage to well-defined irregular figures.

- Porosity comprises rounded cavities or distributions of rounded cavities. It is caused by the freezing of gas bubbles in solidifying molten metal or in solid metal soft enough to be deformed by the pressure of an emerging gas. Indications are dark and may range from shadowed areas for a distribution of microporosity to well-defined circular spots from spherical pores or lines from continuous distributions of pores ('piping porosity,' 'wormhole porosity,' 'or hollow bead').

- Cracks result when stresses within the weld metal exceed the fracture stress capability of the metal. Dynamic thermal stresses acting on hot weld metal produce 'hot cracks'; residual stresses acting on cold weld metal produce 'cold cracks' or 'delayed cracks.' Crack morphology is widely varied. Crack indications on a radiograph are dark, and vary widely with the morphology.

4. DEFINITION OF AN ENIGMA

In a radiographic context, an enigma is an indication from a weld lacking an obvious corresponding structural feature. Enigmas are not usually considered harmful to the integrity of a weld, although the nature of the underlying structure responsible for the enigma must be considered before dismissing it as a harmless indication. Lack of obvious structural characteristic does not guarantee harmlessness. During NDE, it is important to identify enigmas unambiguously. If this cannot be done, the indication must be treated as a defect indication even when its nature as an enigma is suspected. These are two common structural features that produce radiographic enigmas—large grains, where enigmas are generated by diffraction, and segregation, where enigmas are generated by differential absorption of radiation. Although other unobtrusive structural features might conceivably produce enigma indications, the contrast mechanisms by which enigmas are generated are limited to diffraction and differential absorption.

4.1 Diffraction Effects

During radiography, a polychromatic x-ray beam impinges on an object. The transmitted beam induces a chemical transformation in photographic film or affects some other medium to map the transmitted beam intensity over the object. The more intense the transmitted beam, the darker the film will be. Image contrast is due to differences in intensity of the transmitted beam through the cross section caused by variations in absorption of the transmitted beam by the internal structure of the object being examined. The transmitted beam creates a reverse shadow effect on the film, since the intensity of x-ray transmitted is fractionally reduced proportional to the density of the object. The lighter the radiographic image produced, the denser the sample. Cracks or voids absorb less of the transmitted beam and show up on film as dark lines or spots. Welds show up as light regions because of extra metal deposited above and below the surface of the parent metal, presenting more material to absorb the transmitted beam.

Sometimes large grains at appropriate orientations give rise to diffraction effects superimposed on the radiographic image. The structural features of the object generating a diffraction effect are, in general, less critical to weld integrity than the defects that generate absorption contrast effects. But sometimes diffraction effects can masquerade as absorption contrast effects caused by defects. When this occurs and the defect anticipated from the contrast effect is not to be found when the object is cut open, the radiographic effect is classified as a 'ghost' or 'enigma.' It should be noted that relatively harmless segregates may also cause indications suggesting defects. Not all enigmas are diffraction effects.

An x-ray radiograph for a polycrystalline material may be compared to a transmission Laue diffraction pattern with only the central transmitted spot observed. This is because for the usual polycrystalline object, Laue diffraction effects cancel out, producing only one transmitted spot. But sometimes large grains, or dendrites in fusion welds, are present and diffraction patterns emerge because of the polychromatic source. A diffracted beam produces an image of the diffracting body. The image is shifted with respect to the transmitted image by the diffraction angle. The intensity of radiation is reduced in places vacated by the diffraction image and increased in places entered by the diffracted image. This produces shadowing effects around the diffraction image. This diffraction produces light and dark

contrasts on opposite sides of the diffraction image of the diffracting grain because the diffracted image adds or subtracts from either side. Figure 1 shows an example of such a diffraction pattern.
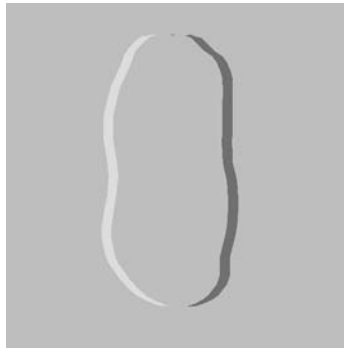
Figure 1. A schematic enigma around a large grain; light and dark regions on either side are due to diffraction.

4.2 Segregation Effects

As a beam of radiation passes through a body, the intensity of the beam diminishes, some of the beam being converted into heat and some diffracted away from the direction of the penetrating beam. The intensity (I) of the beam drops with distance traveled (x) according to the relation $dI/dx = -\mu I$, where μ is the absorption coefficient for the beam. If a hole or crack exists in a material, it acts as a spot of reduced absorption for any beam crossing it, and raises the transmitted x-ray intensity so as to become visible as a dark (more exposed) indication on detecting film. If, instead of a hole, there is a region of elemental segregation in a material, the absorption coefficient can be either lower or higher, producing a dark or light indication, depending on the density differences between the segregated element and the surrounding material.

Segregation occurs during solidification from a melt. As the freezing interface moves forward, the newly formed solid ejects solute into the liquid phase. As freezing progresses, both newly solidified solid phase and the remaining liquid phase take on higher concentrations of solute. Typically, this kind of segregation manifests itself on a small scale and is not likely to be visible at the macroscale of a radiograph. In micrographs, polished and etched dendrites are clearly visible. The interdendritic metal being more highly alloyed tends to be attacked more vigorously by an etch. Hence, the interdendritic etched surface tends to be rougher than that of the dendrite core and tends to be darker in bright field contrast.

If, however, a partially solidified metal is subjected to pressure, the pressure can drive the remaining liquid phase with its relatively high solute concentration to migrate on a macroscopic scale. Thermal stresses in welds may produce such pressures. The resultant segregation structure may produce variations in transmitted x-ray intensity and produce visible indications on detecting film. Such segregation structures are not usually considered harmful to the integrity of a weld and their indications are usually classed as enigmas. It is necessary to be cautious, however. Second phase coarsening, suggesting

segregation as described above, has been found at the toes of GTAW welds. This may correlate with a reduction in strength of welds with intact reinforcements. Pending further study, this might explain why, in some cases, the removal of weld reinforcements increases weld strength. The actual drop in strength here is not attributed to segregation per se, but rather to the associated coarsening of a phase.

5. EXPERIMENTAL SETUP

5.1 Welding

An Automated Manufacturing Engineering Technologies (AMET) GTAW system was used to join 12-in-long × 6-in-wide × 0.05-in-thick Inconel 718 panels with a single-pass butt weld. The setup is shown in figure 2 and weld settings for the subsequent experiments can be found in appendix A. A camera was set up to video record in situ weld puddle variations behind the torch during experiments.
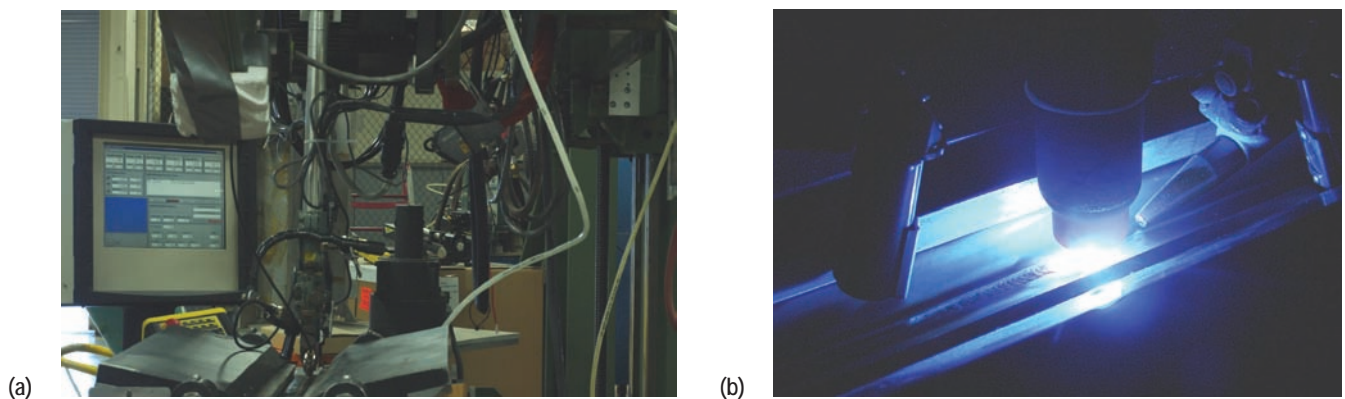
Figure 2. Weld setup with (a) the AMET system and (b) clamping fixture.

A first set of experiments was conducted to determine the nominal parameters using bead-on-plate welds both with and without filler wire. After observations of video footage of the weld operations, it was concluded that for ease of visibility, filler wire would be used for the subsequent joint welds. No radiography was conducted on the bead-on-plate experiments.

Using the bead-on-plate experiments as a starting point for nominal settings, it was decided that variations in travel speed would be used to manipulate the weld puddle shape. A second set of experiments determined travel speed variations for round, oval (nominal), and tear-drop-shaped puddles.

Finally, separate panels were welded together in a joint with variations in cross-slide displacement, and then with variations in current to produce lack of fusion and lack of penetration, respectively. This was done so that a comparison could be made between enigma and defect radiographic indications. A table of weld parameters for each joint pass is located in appendix A. No heat treatment was conducted on any of the weld panels for this experiment.

5.2 Nondestructive Evaluation Procedures and Sample Preparation Methods

Radiographic NDE was conducted on all of the joint panels (JT-01 through JT-09). On several of the panels, multiple radiographs were taken to determine if differences in x-ray orientation (±10° off perpendicular) produced any differences in size, clarity, or location of the parallel linear indication.

NDE standards say that all areas of interest should be x-rayed such that the film density, determined with a densitometer, is between two (1% light transmission) and four (0.01% light transmission).[7] The density of the film is the base-10 logarithm of the intensity of the incident light from a densitometer source divided by the transmitted intensity. If all areas of interest cannot be displayed in a single picture, then multiple x-ray images should be taken. This is particularly important since the welded area is much denser than the parent metal, making it difficult to inspect for cracks, or missed joint indication in both parent metal and welded area with the same radiograph. It is important to note, that except for JT-08, the film density requirements standards were not followed.

Qualitative eddy current testing was conducted on the enigma panel and the two defect panels for comparison of results. Penetrant testing was conducted on the lack-of-fusion weld (JT-08).

Sections of the weld joint were then selected for microscopic observations based on nominal radiographic conditions seen along the length of the weld. Samples, as shown in figure 3, were cut and mounted to produce images of the crown and transverse surfaces of the weld. Samples were then mechanically polished and electrochemically etched to reveal microstructural features including grain boundaries, and the interface between weld and parent metal.

Crown   Transverse
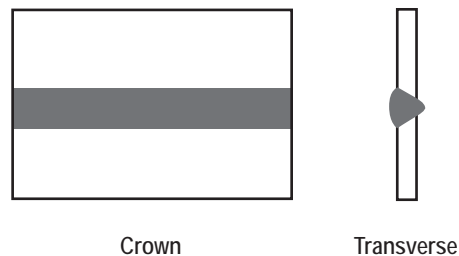
Figure 3. Weld sample cut prior to mounting, polishing,
and etching to reveal structure.

6. OBSERVATIONS

Puddle shape is determined by the ratio of the speed at which the puddle edge freezes to the rate at which the weld heat source is moved; i.e., the weld travel speed. When the freezing rate of the weld metal is appreciably faster than the weld travel speed, the back edge of the weld puddle easily keeps up with the travel speed and the back edge of the puddle is round. When the freezing rate of the weld metal is appreciably slower than the weld travel speed, the molten metal extends back from the weld heat source and the puddle edges move in from the sides along straight lines, ending in a point and marking out a tear-drop shape for the weld puddle. Between these two extremes, the weld puddle takes an elliptical shape. Travel speed, from 2 in/min to 7.5 in/min, greatly changed the appearance of the molten weld puddle.

The round weld puddle, as seen in figure 4(a), was a feature of slowest travel speed (JT-03), and was accompanied by excessive root reinforcement and minimal crown reinforcement. This was also the largest of the weld puddles, with the puddles getting progressively smaller as the travel speed increased and heat input per unit length of weld decreased.

During the nominal weld settings (JT-02), the welders observed an oval-shaped weld puddle (fig. 4(b)) and postweld inspections showed an appropriate amount of reinforcement.

The tear-drop weld puddle (fig. 4(c)) was created using the fastest travel speed (JT-04). It had excessive crown reinforcement and little root reinforcement, in contrast to the round weld puddle. Also, mismatch caused by inadequate clamping forces from the fixture was seen near the end of several panels, most noticeable on panel JT-05. Reduced puddle size at the faster travel speeds made it easier to identify joint mismatch.

(a)   (b)   (c)

Figure 4. Differently shaped molten puddles: (a) round (JT-03), (b) oval (JT-02),
and (c) tear-drop (JT-04). The label BACKSIDE denotes that weld direction
is upward, that the observer is looking behind the weld puddle.

The radiographic images showed that the slower the travel speed, the more prevalent the linear enigma indications were, both in the radial direction and the direction parallel to the joint. The slowest travel speed, the one with the most heat input, produced substantial linear indications parallel to the joint

and radial indications on either side of the parallel indication as shown in figure 5. The radiographs from the nominal weld speed showed only radial indications (fig. 6). These radial indications are caused by columnar grain structures with a dendritic core elongated in the direction of solidification. The fastest travel speed produced no radiographic linear or radial indication (fig. 7).

(a)

(b)
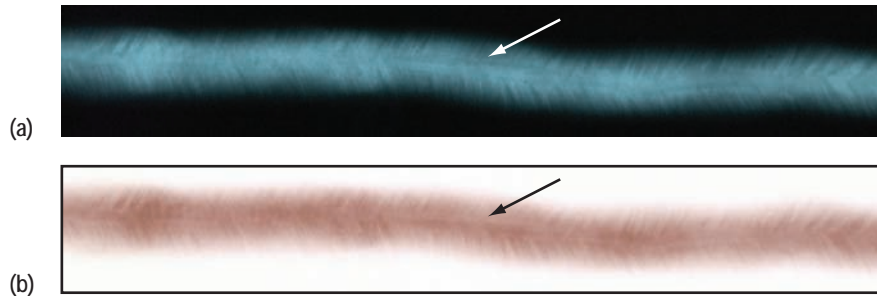
Figure 5. Round-puddle weld (JT-03) showing (a) radiographic and (b) reverse contrast images. Notice the linear indication running the length of the weld pointed out by the arrows, and the radial feathering indications of columnar grains on either side. Weld direction is from right to left.

(a)

(b)
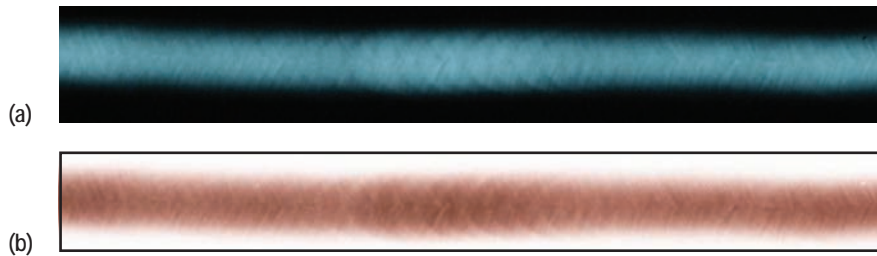
Figure 6. Nominal weld (JT-02) showing (a) radiographic and (b) reverse contrast images. Notice the radial feathering indications caused by columnar grain formation. Weld direction is from left to right.

(a)

(b)
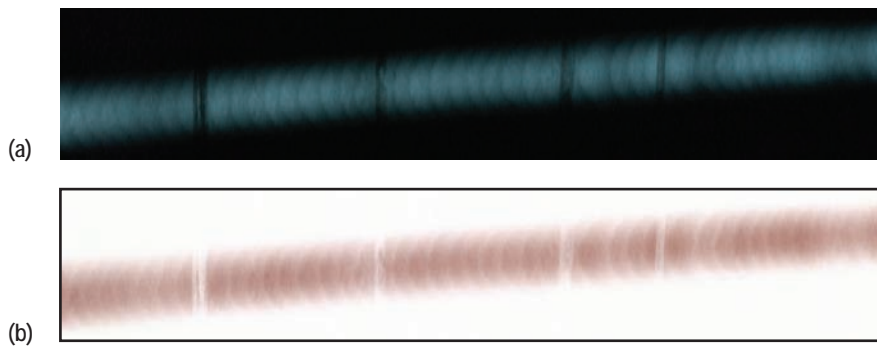
Figure 7. Tear-drop weld (JT-04) showing (a) radiographic and (b) reverse contrast images; no visible lateral indications or linear indications. Vertical lines are grease pencil markings. Weld direction is from left to right.

The radiographs seen in figure 8 were then taken of JT-03 with the x-ray source oriented at ±10° to the original perpendicular position. The three different x-ray source angles produced three different images at the same location in the weld joint. The indications never disappeared or changed location, but they did change size and clarity. Measurements on overall thickness of the indications were taken and summarized in table 2. They showed that the thickness of the linear indication increased as the x-ray source was moved from –10° to 0° to +10° orientations.

(a)

(b)

(c)
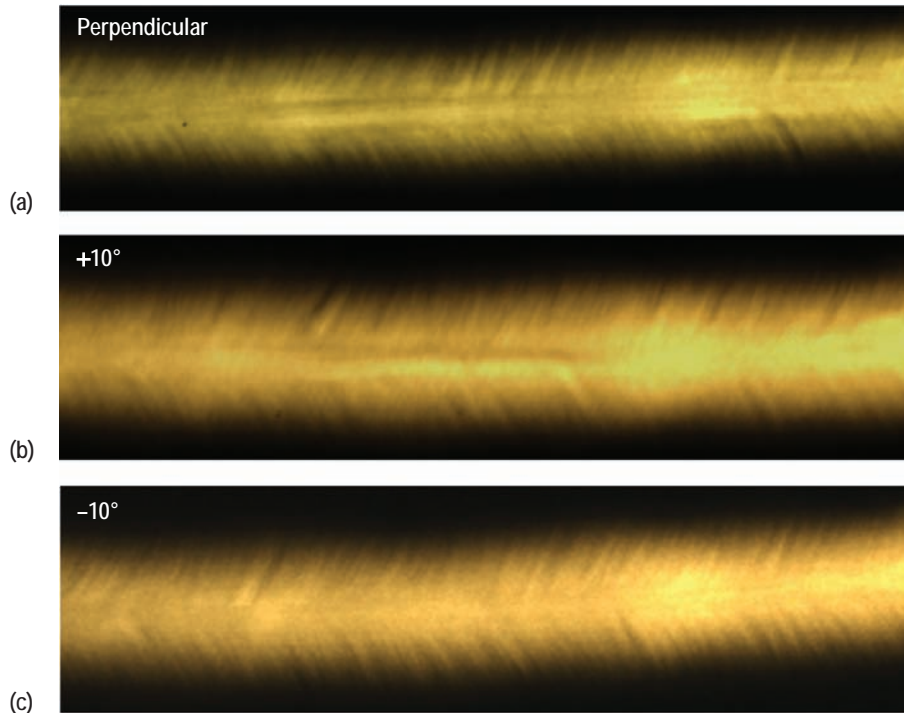
Figure 8. Radiographic images of JT-03. The x-ray source was oriented: (a) perpendicular, (b) +10°, and (c) –10° to the weld panel. The contrast between the dark and light indications changes with the x-ray source orientation. Weld direction is still right to left.

Table 2. Linear indication width (inches) at three locations on the radiographs.

Radiograph Location (in)	X-ray Orientation to Panel		
	−10°	0°	10°
2	0.0071	0.0079	0.0087
6.5	0.0047	0.0055	0.0071
9	0.0039	0.0055	0.0063

The slowest travel speed (JT-03) was cut into macros at two locations—one where the linear indications parallel to the joint were easily defined as a dark and light line pair (JT-03_1) and the second in a location where there was only one grey indication (JT-03_2). The macros from both locations showed that longitudinal columnar dendrite structures were formed parallel to the joint, which was easy to see in the crown macros in figures 9 and 10. The transverse cross sections show that at the JT-03_1 location (fig. 11) columnar dendrites are lined up through the depth of the weld, with a consistent boundary and thickness through the depth of the weld. In contrast, the transverse macro from JT-03_2 showed that the boundaries between parallel columnar dendrites and the rest of the weld nugget are not parallel to each other and the region's thickness is also not consistent through the depth of the weld as seen in figure 12.

Figure 9. Crown macro of JT-03_1 region. In the center is a long grain with a substructure of dendrites. The weld direction is from top to bottom.
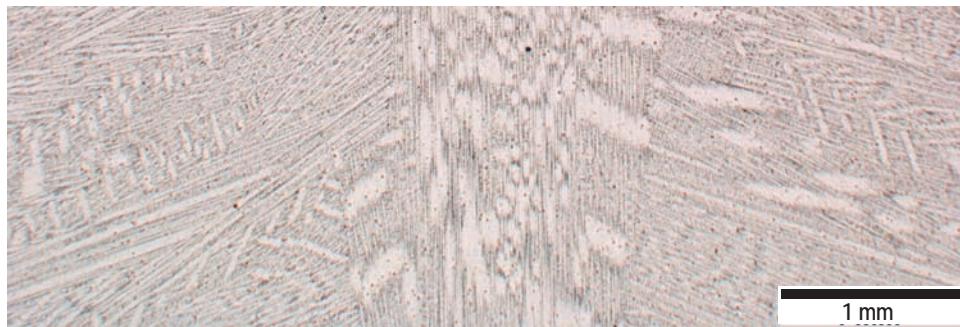
Figure 10. Crown macro of JT-03_2 region. The linear region in the center is a grain comprised of dendrite formations. The weld direction is from bottom to top.
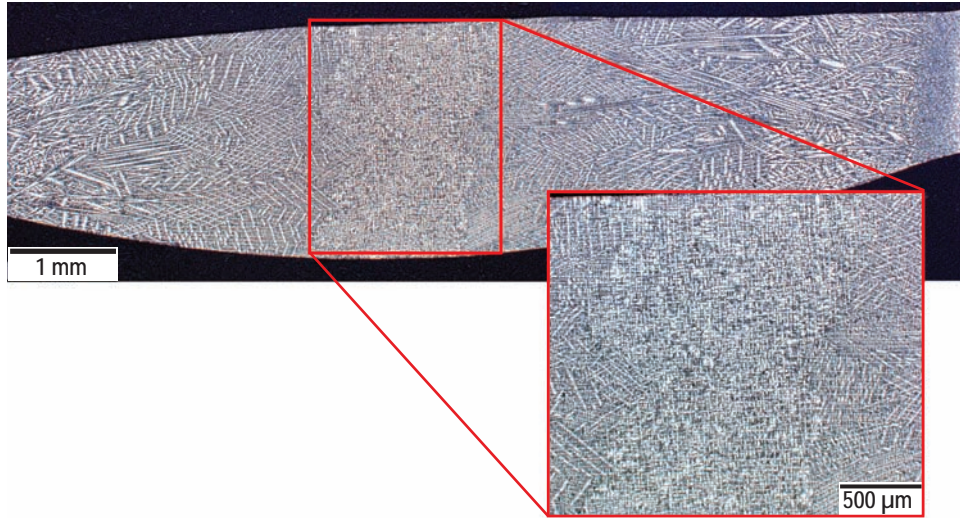
Figure 11. Transverse macro of JT-03_1. Notice that the large dendrite structure (grain) in the center extends through the depth of the weld. Crown side is up.
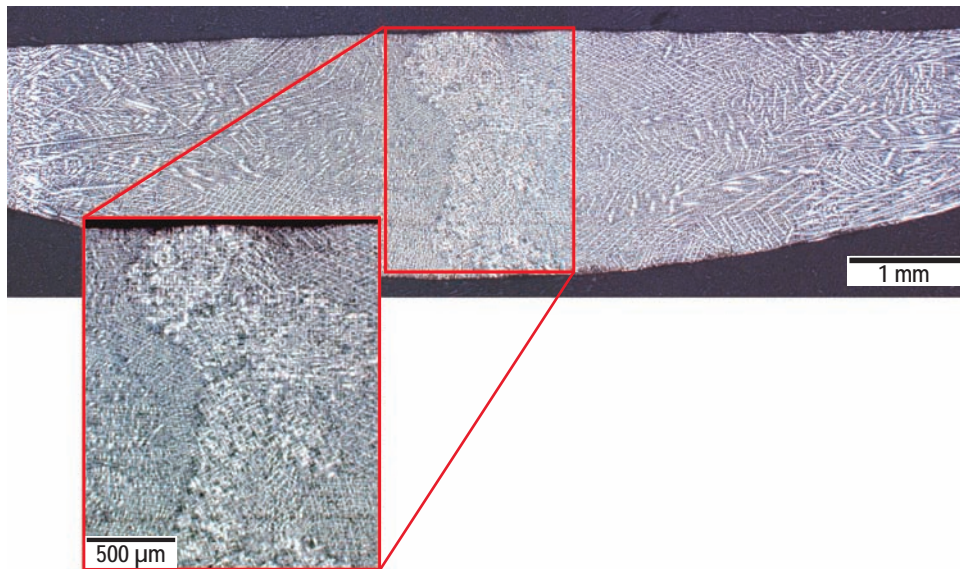
Figure 12. Transverse macro of JT-03_2. Notice that the center of the weld lacks a consistent large dendritic structure (grain) extending through the weld as seen in figure 11. Crown side is up.

The crown macro (fig. 13) for the nominal weld speed (JT-02) shows that the lateral dendrite formations come together at the center of the weld and create a disjoint microstructure in the absence of any longitudinal dendrite formations. At higher magnification (fig. 14), it can be seen that these dendrites produce a visible boundary. This implies that the weld speed is somewhat higher than the rate of freezing, even though the puddle appeared to have an elliptical shape with a flat perimeter at the trailing edge.
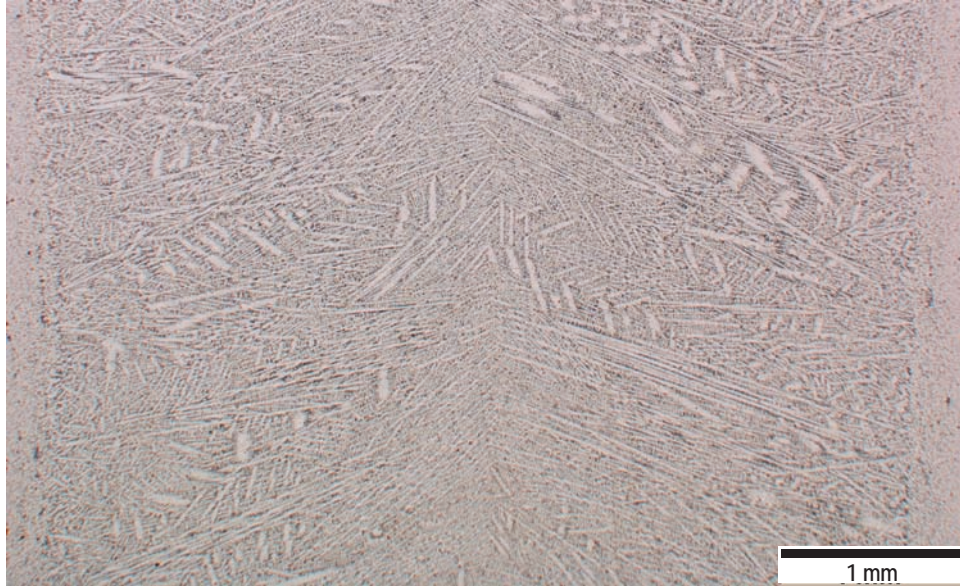
Figure 13. Crown macro of JT-02, nominal weld speed. The lateral dendrites meet with almost disjoint mirror symmetry at the center of the weld joint.
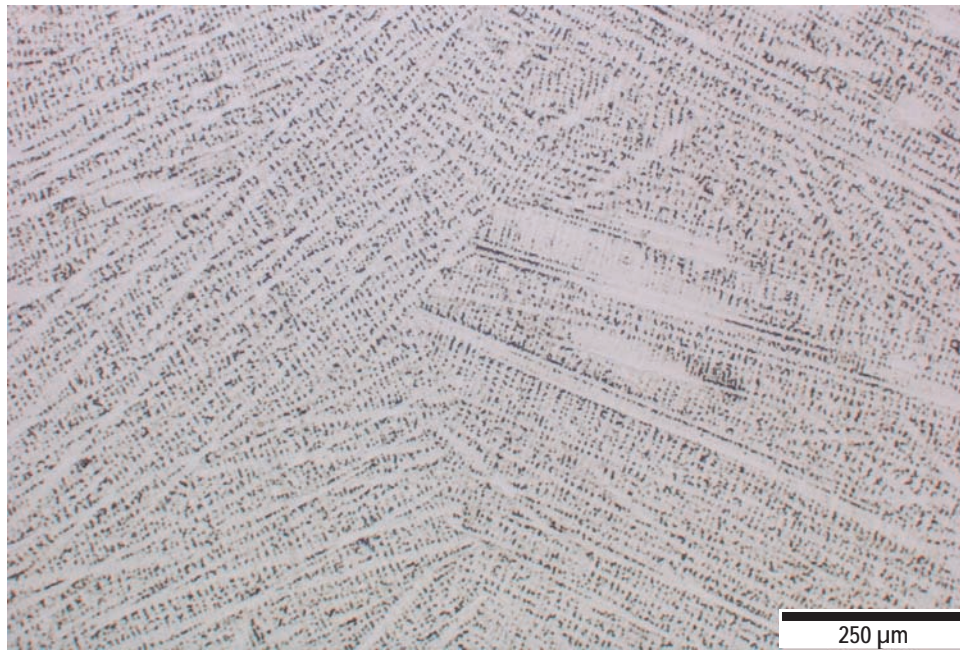
Figure 14. Crown macro enlarged of JT-02, nominal weld speed. Notice conjunction of lateral dendrites at the center of the weld. The weld direction is from bottom to top.

The crown macro for the tear-drop weld speed (JT-04) shows a random equiaxed dendrite orientation (fig. 15). The higher magnification (fig. 16) verifies this random configuration. The relatively high solidification velocity of the fastest weld speed apparently does not allow time for columnar formation since the transformation kinetics of the Inconel 718 structure is slow.

Figure 15. Crown macro of JT-04. Notice there is no relative orientation preference for the dendrite formations. Notice that weld direction is indiscernible for this joint.

Figure 16. Crown macro enlarged of JT-04. Notice there is no relative orientation preference for the dendrite formations.

16

Subsequent weld experiments were conducted to produce mismatch, lack of fusion, and lack of penetration indications.

By varying the clamping pressure on the panels during welding, the welders were able to produce a joint with significant mismatch, near the end of the panel. From the radiographic image (fig. 17), it can be seen that this mismatch created an indication in the form of an ~0.01-in light and dark region on either side of a boundary running approximately along the middle of the weld. The macro image of figure 18 explains the indication. The crown is flat, but there is a step at the weld root, such that the thickness penetrated by the x-ray beam is significantly different on opposing sides of the step.
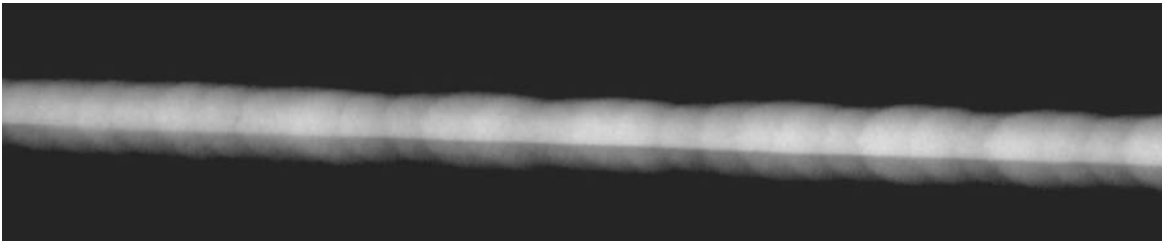
Figure 17. Radiographic image of JT-05. The mismatch indication can be seen as a light image with a darker image superimposed over the lower part of the weld. Weld direction is left to right.

Figure 18. Transverse macro of JT-05. Notice the visible mismatch on the root side.

The lack of fusion weld was created by cross sliding the weld puddle until the joint was seen just at the edge of the crown reinforcement (fig. 19). The radiograph showed a blurry dark line at the position where the cross slide moved the bead back to the middle of the joint (fig. 20) but there was no visible indication for the remaining length of the missed joint. The macro shows that there was almost complete lack of fusion for the length of the joint (fig. 21). Penetrant testing was conducted on JT-08 and produced visible porosity indications on the root side of the weld along the length of the joint.

Figure 19. Segment of weld JT-08. The bead has been displaced toward the right until it has been moved almost off the joint (see transverse section fig. 21), which can be seen extending from the left edge of the bead. At this point, the joint is only being partially consumed by the weld bead.

(a)

(b)
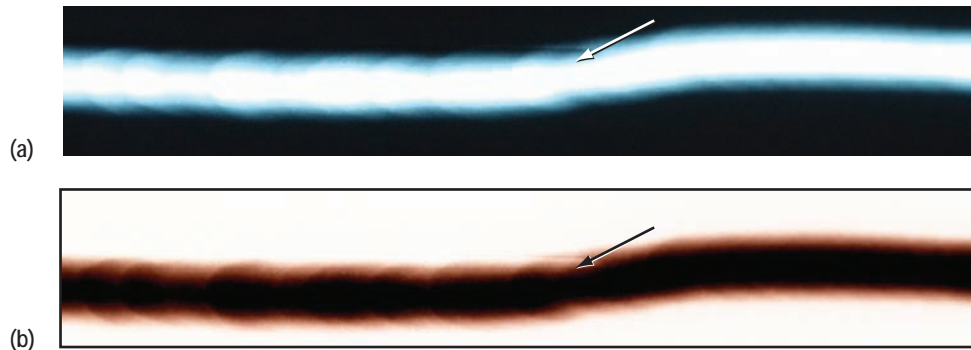
Figure 20. Radiographic image of JT-08 showing lack of fusion at the arrow where the cross-slide motion was used to move the bead back toward the center of the joint: (a) is the radiographic image; (b) is the reverse contrast image. Under the radiographic contrast conditions shown, the unwelded joint extending to the left from the visible indication is not visible. Weld direction is from left to right.

Figure 21. Transverse macro of weld JT-08, where a missed joint can
be seen on the left side of the image. The crown is on the top.

X-rays of JT-08 were also taken at ±10° of the original x ray. The –10° panel did not show a linear indication for the lack of fusion, but it did produce a linear enigma indication near the beginning of the weld that was not observed of either the perpendicular or +10° radiograph (fig. 22). The +10° panel showed a dark linear indication produced by the lack of fusion under the crown reinforcement along the length of the weld (fig. 23).
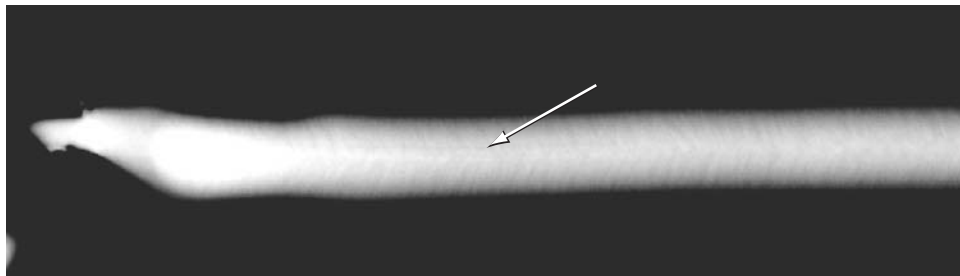
Figure 22. Radiograph of JT-08 taken at –10° off perpendicular. A faint enigma
indication can be seen near the start of the weld joint. Weld direction
is left to right.
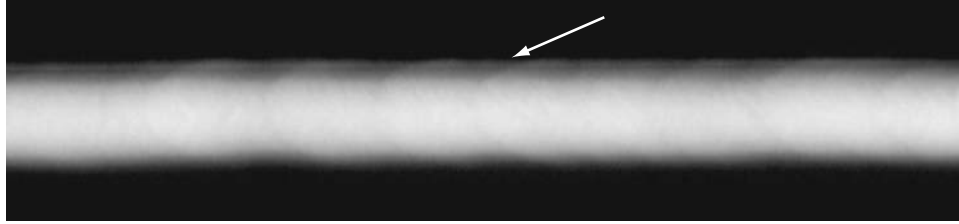
Figure 23. Radiograph of JT-08 taken +10° off perpendicular. The linear indication caused by lack of fusion can be seen along the top of the crown reinforcement. Weld direction is left to right.

When the proper radiographic standards are followed, and the image density of the parent metal is within the 2 to 4 density range, the missed joint is clearly visible in the radiograph taken perpendicular to the joint (fig. 24).
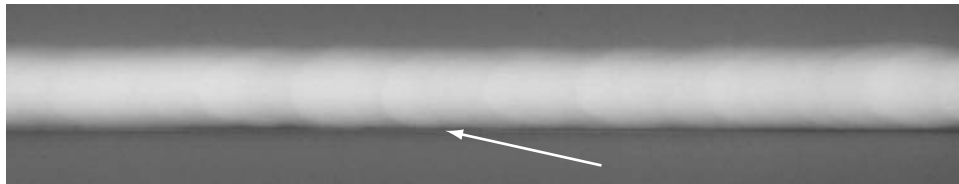
Figure 24. Radiograph of JT-08 with x-ray source oriented perpendicular to the joint. The lack of fusion, missed joint can be seen as a blurry dark line along the bottom of the image. This image has been reversed with respect to the previous image.

Lack of penetration in the center of the weld joint was created by reducing the weld current enough to decrease the penetration depth while still maintaining a stable puddle. Lack of penetration in weld JT-09 produced a dark indication of the weld joint (fig. 25(b)). X-ray orientations at ±10° of perpendicular produced the radiographs seen in figure 25(a) and (c), respectively. The linear indication moved up and down, above and below the center of the weld joint, but did not change intensity or appearance appreciably at these low angle change increments. Figure 26 shows the lack of penetration responsible for these indications.
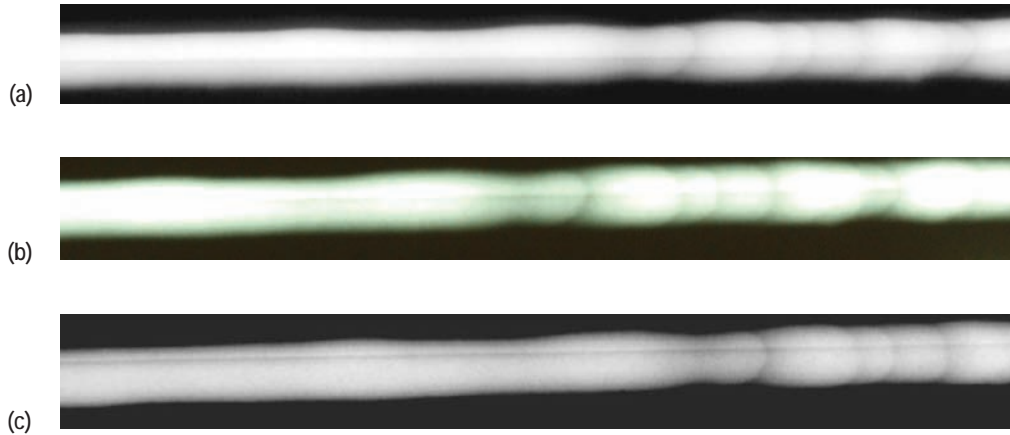
Figure 25. A comparison of radiographs with x-ray source at (a) +10°, (b) perpendicular, and (c) –10°. Notice that the linear indication caused by lack of penetration moves in the weld puddle but does not substantially change clarity or size. Weld direction is right to left.
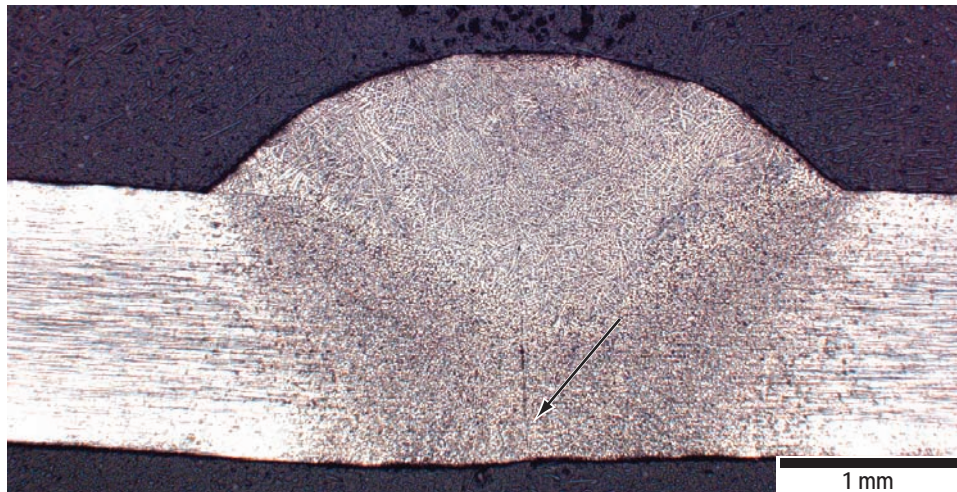
Figure 26. Transverse macro of JT-09. The lack of penetration can be seen in the center of the weld near the root side.

Eddy current testing, using a two-coil probe, was conducted on panels JT-03, JT-08, and JT-09. The linear dendrite formations that caused the enigma indication in JT-03 produced no eddy current indications and passed inspection. Lack of fusion and lack of penetration as exhibited by JT-08 and JT-09, respectively, did not pass eddy current inspection. JT-08 produced an indication, but the operator was unsure about the size of the defect causing the indication. The eddy current data were representative of either a very shallow and/or narrow defect running the length of the weld on the root side. The eddy current data for JT-09 indicated a narrow root side lack of penetration along the center of the weld. On both JT-08 and JT-09 indications were produced only when the eddy current probe was located on the root side of the weld joint. The depth of field of the eddy current probe makes it only possible to detect surface flaws.

7. MECHANICAL PROPERTIES

In order to provide a standard of comparison for tensile tests of the weld joints described above, tests were first conducted on the parent metal, which was certified by chemical analysis to be Inconel 718. Parent metal tensile test data are compared to tensile test data for nonheat-treated Inconel 718 in table 3. The parent metal was comparable to the strength specifications for nonheat-treated Inconel 718; i.e., 2-percent yield of 140 ksi maximum and tensile strength of 80 ksi maximum.

Table 3. A comparison of reference tensile properties and experimental properties of parent metal and welded specimens.

		Specimen ID	UTS (ksi)	Yield Strength (ksi)	Plastic Strain (%)	Comments
AMS 5596J Specs		–	Max: 140	Max: 80	30	Plastic strain not comparable with experimental
Parent Metal		PAR-1	137.918	65.21	23.132	–
		PAR-2	121.433	62.21	22.945	–
		PAR-3	130.276	62.047	22.872	–
		PAR-4	144.649	70.01	23.085	–
Weld Panels	JT-02: Nominal Oval	02-O-1	133.326	64.506	22.885	Fractured in parent material away from weld
		02-O-2	133.93	64.719	23.002	Fractured at edge of weld nugget
		02-O-3	132.053	54.825	22.71	Fractured in parent material away from weld
	JT-03: Enigma Round	03-R-1	128.484	62.488	23.065	Fractured at edge of weld nugget
		03-R-2	127.957	60.677	22.898	Fractured at edge of weld nugget
		03-R-3	134.458	55.65	22.793	Fractured at edge of weld nugget
	JT-04: Fast Tear-Drop	04-T-1	135.071	64.888	22.885	Fractured in parent material away from weld
		04-T-2	134.728	64.507	22.977	Fractured in parent material away from weld
		04-T-3	135.403	59.929	22.937	Fractured in parent material away from weld

Samples from welds JT-02, JT-03, and JT-04 were tested; results are listed in table 3 to determine if the enigma indications caused by columnar dendrite formations decreased the integrity of the weld. No specimens from welds JT-05, mismatch; JT-08, lack of fusion (missed joint); and JT-09, lack of penetration, weld joints were tested since these did not pass initial radiographic inspections.

All the specimens from weld JT-03 and one of the specimens from JT-02 fractured in the heat-affected zone of the weld. All the other failures were located in the parent metal. Average and standard deviation for the tensile properties of the weld joints and parent metal are listed in table 4.

22

Table 4. Statistical results of the tensile data.

	Average UTS (ksi)	Std Dev UTS (ksi)	Average Yield (ksi)	Std Dev Yield (ksi)	Average Plastic Strain (%)	Std Dev Plastic Strain (%)
Parent Metal	133.57	10	64.87	3.72	23.01	0.12
JT-02	133.1	0.96	61.35	5.65	22.87	0.15
JT-03	130.3	3.61	59.61	3.54	22.92	0.14
JT-04	133.36	3.48	63.11	2.76	22.93	0.05
Nugget Edge Fracture	131.21	3.46	60.88	3.86	22.94	0.12
Parent Mat Fracture	134.12	1.4	61.73	4.37	22.88	0.1

As the welds range from slower to faster, JT-03 → JT-02 → JT-04, the average UTS rises slightly, 130.3 ksi → 133.1 ksi → 133.4 ksi. If standard deviation error bars are placed on the data, 126.7–133.9 ksi →132.1–134.1 ksi → 129.9–136.9 ksi, there is a window of commonality from 132.1 to 133.9 ksi. Nevertheless, if a small but not quite insignificant reduction in strength for the slowest welds is accepted, might it be attributed to a slightly altered microstructure caused by longer exposure to high temperature or to the enigma generating central grain structure, both features being associated with the slowest speeds?

Fractures at the edge of the weld nugget occurred in slow welds exhibiting enigma indications, but also in one weld at nominal speed lacking the large central columnar grains associated with enigma indications. This points to general microstructural alteration rather than large central grains as the key factor in any reduction in strength at slower weld speeds. Given the present mechanical property data there is no evidence that enigma-producing large grains per se reduce the strength of welds significantly. Enigmas may, however, signal a small collateral reduction in weld strength due to microstructural changes associated with longer exposure to high temperatures.

8. CONCLUSIONS

The following conclusions were reached:

(1) The slower the travel speed, the easier it is for the freezing rear of the weld puddle to keep up with the puddle motion and for columnar grains to propagate from the rear of the weld along the weld bead center.[6] Columnar grain structures entering the puddle from the sides (radial feathering) are also coarser and more visible at slower travel speed:

• The central columnar grain and corresponding linear enigma indications in the radiographic image were observed with slow speed weld JT-03. Also visible was pronounced radial feathering.

• No central columnar grain or central enigma indication was observed with nominal speed weld JT-02. Radial feathering was visible normal to the weld bead surface contours.

• Only weld bead surface contours were observed with high-speed weld JT-04.

• Enigma indications were also visible in the –10° image of JT-08, which was welded at nominal setting with a cross slide displacement.

(2) The enigma indications (JT-03 and JT-08) changed size with relation to the angle of the x-ray source but did not change location, and followed patterns associated with deflection of the x-ray beam through an aligned structure. Appendix B relates the width of enigma line indications to x-ray source angle due to diffraction effects (but not due to contour effects of the diffracting body).

(3) Enigma indications were either a distinct dark and light line pair or a gray blurry line in the center of the weld joint. Both indication types were similar in intensity to that of the weld reinforcement. The differences in the clarity of these indications are caused by variations in width of the columnar dendrites through the thickness of the weld joint. Formations that are consistently vertical through the thickness of the weld produce clearer indications than formations with slanted boundaries.

(4) Mismatch produced a radiographic image in which half the weld joint appeared darker than the other half of the weld joint.

(5) Lack of fusion, or a missed weld joint, produced a wide black linear indication which was substantially different in intensity from those associated with nominal variations of weld density. Small variations in x-ray source location moved this indication in and out of view but the indication size and clarity did not change. When the joint was radiographed at reduced exposure so that the parent metal was visible, the lack of fusion indication was easily observed. Penetrant inspection produced indications of porosity at the location of the missed weld joint.

(6) Lack of penetration in the center of the weld produced a sharp black linear indication which was substantially different in intensity from those produced by variations of weld density. Small variations in x-ray source location moved this indication in and out of view but the indication size and clarity did not change.

(7) Eddy current did not produce any defect indications with the enigma. Eddy current has a difficult time in detecting lack of fusion when the joint is pulled together tightly, producing only a narrow crack. It correctly indicated the location of the lack of penetration, but was unable to assess the depth of the defect. Eddy current's lack of depth of field makes it so that an indication is only produced if the probe is located on the same side as the defect. This means that defects on the root side of the weld, in a tube, would need to be inspected from inside the tube to get eddy current results. This technique also requires more time than radiographic imaging. Eddy current is not judged to be a good candidate for NDE inspections of welds.

(8) Tensile testing did not reveal a statistically significant difference in weld strength between welds exhibiting enigma indications and the as-received condition of Inconel 718. Further testing should be conducted to determine if postweld heat treatment and aging affects the performance of the worst-case enigma joint (JT-03).

With the understanding of how defect indications and enigma indications behave when radiographed, a set of guidelines can be created to help the inexperienced radiographer determine the origin of a linear defect. A categorized set of known indications can help in both training applications and decreasing onsite misinterpretations.

9. RECOMMENDATIONS FOR DISTINGUISHING RADIOGRAPHIC ENIGMA INDICATIONS FROM DEFECT INDICATIONS

The present recommendations pertain to recognizing enigma indications in butt welds in Inconel 718, but may be applied *mutatis mutandis* to other situations involving enigmas:

- Consider from past experience and from processing physics whether an enigma indication is likely to be present.

- Observe the details of the image under consideration for compatibility with enigma and defect images observed and computed from theory.

- Observe whether multiple radiographic images generated at different incident beam angles vary in conformity with expectations for an enigma or for a defect.

The experimental enigma and defect indications generated herein and the discussion of the formation of the diffraction image enigma are intended as aids in carrying out the above recommendations. Experienced radiographic observers do something like this implicitly, but implicit procedures are subject to incompleteness and carelessness and to latent undue influence by desired outcome. Implicit analyses are not adequate for explaining the basis of a judgment call to others. When decisions are critical, explicit analyses are preferable.

APPENDIX A—WELD SETUP

WELD DATA SHEET

PARENT METAL: Inconel 718   THICKNESS: 0.05 inch
PROCESS: TIG   POSITION: Flat

TORCH TYPE: HW-27   POWER SUPPLY: AMET   FIXTURE: horizontal
SHIELD CUP SIZE: #12   SIZE   TIP CONFIGURATION: tapered
TUNGSTEN TYPE: 2% thoriated   SIZE: 3/32 inch
LEAD ANGLE: 3 degrees
SHIELD GAS TYPE: Argon   FLOW: 50 CFH
BACK GAS TYPE: Helium   FLOW: 100 CFH
FILLER WIRE TYPE: Inconel 718   SIZE: 0.04 inch
PRE_WELD PREP: Grind w/320 grit SiC, Acetone wipe
NOTES: The above settings were not changed between panels.

PANEL NUMBER: JT-01
AMPS: 60   VOLTS: 8.2   TRAVEL: 5 ipm
WIRE SPEED: 10 ipm   CROSS SLIDE: 0
NOTES: Irregular puddle shape due to low voltage. Setting determined from bead on plate welds (BP-01-05).

PANEL NUMBER: JT-02
AMPS: 60   VOLTS: 8.5   TRAVEL: 5 ipm
WIRE SPEED: 10 ipm   CROSS SLIDE: 0
NOTES: Puddle shape became regular with increase in voltage. SHAPE: oval.

PANEL NUMBER: JT-03
AMPS: 60   VOLTS: 8.5   TRAVEL: 2.5 ipm
WIRE SPEED: 10 ipm   CROSS SLIDE: 0
NOTES: Increased solidification time by increasing heat input. SHAPE: round.

PANEL NUMBER: JT-04
AMPS: 60   VOLTS: 8.5   TRAVEL: 7.5 ipm
WIRE SPEED: 10 ipm   CROSS SLIDE: 0
NOTES: Raised puddle, smaller penetration zone. SHAPE: tear-drop

PANEL NUMBER: JT-05

AMPS 55 VOLTS 8.5 TRAVEL 7.5 ipm

WIRE SPEED 10 ipm CROSS SLIDE 0

NOTES: Tried to achieve LOP or LOF. Visual inspection does not show LOP.

PANEL NUMBER: JT-06

AMPS 60 VOLTS 8.5 TRAVEL 7.5 ipm

WIRE SPEED 10 ipm CROSS SLIDE 0.025 in

NOTES: Tried to achieve LOP or LOF. Visual inspection does not show LOP.

PANEL NUMBER: JT-07

AMPS 60 VOLTS 8.5 TRAVEL 5 ipm

WIRE SPEED 10 ipm CROSS SLIDE 0.05 in

NOTES: Tried to achieve LOF coupled with solidification lines. Visual inspection does not show LOF.

PANEL NUMBER: JT-08

AMPS 60 VOLTS 8.5 TRAVEL 5 ipm

WIRE SPEED 10 ipm CROSS SLIDE 0.101in

NOTES: Tried to achieve LOF coupled with solidification lines. Visual inspection does show LOF.

PANEL NUMBER: JT-09

AMPS 50 VOLTS 8.8 TRAVEL 6 ipm

WIRE SPEED 10 ipm CROSS SLIDE 0

NOTES: Tried to achieve LOP and solidification. Visual inspection shows possible LOP.

PANEL NUMBER: BP-01

AMPS 60 VOLTS 8.2 TRAVEL 5 ipm

WIRE SPEED 10 ipm CROSS SLIDE 0

NOTES: Camera movement caused variations in weld puddle. Retry setting on BP-02 to be certain.

PANEL NUMBER: BP-02

AMPS 60 VOLTS 8.2 TRAVEL 5 ipm

WIRE SPEED 10 ipm CROSS SLIDE 0

NOTES: Nominal settings produced a stable oval puddle shape.

PANEL NUMBER: BP-03

AMPS 60 VOLTS 8.2 TRAVEL 5/2.5/7.5 ipm

WIRE SPEED 10 ipm CROSS SLIDE 0

NOTES: Variations of travel speed produced oval/round/tear-drop puddles.

PANEL NUMBER: BP-04

AMPS 60 VOLTS 8.2 TRAVEL 5 ipm

WIRE SPEED 0 ipm CROSS SLIDE 0

NOTES: Nominal settings without wire feed. Puddle shape is more difficult to determine.

PANEL NUMBER: BP-05

AMPS 60 VOLTS 8.2 TRAVEL 5/2.5/7.5 ipm

WIRE SPEED 10 ipm CROSS SLIDE 0

NOTES: Variations of travel speed produced oval/round/tear-drop puddles. Difficult to see puddle shape.

APPENDIX B—TRANSFORMATION OF DIFFRACTION ENIGMA IMAGES

B.1 Effect of Tilting the Beam

Given a point $h00$ in the reciprocal lattice of a crystal of lattice parameter a, figure 27 shows the condition for a reflection from an x-ray beam containing a range of wavelengths.[8] For the point to be on the reflecting sphere, the component of the beam with wavelength λ is selected.

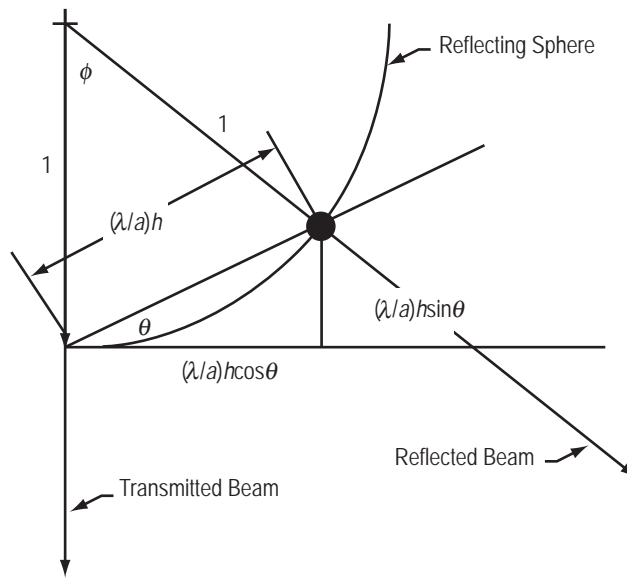Figure 27. Diffraction condition for reflection from reciprocal lattice point $h00$.

The angle of the reflected beam (ϕ) varies with the angle of the reciprocal lattice (θ) with respect to the transmitted x-ray beam (fig. 28) according to the relations:

$$\cos\phi + \frac{\lambda}{a}h\sin\theta = 1$$

$$\sin\phi = \frac{\lambda}{a}h\cos\theta$$

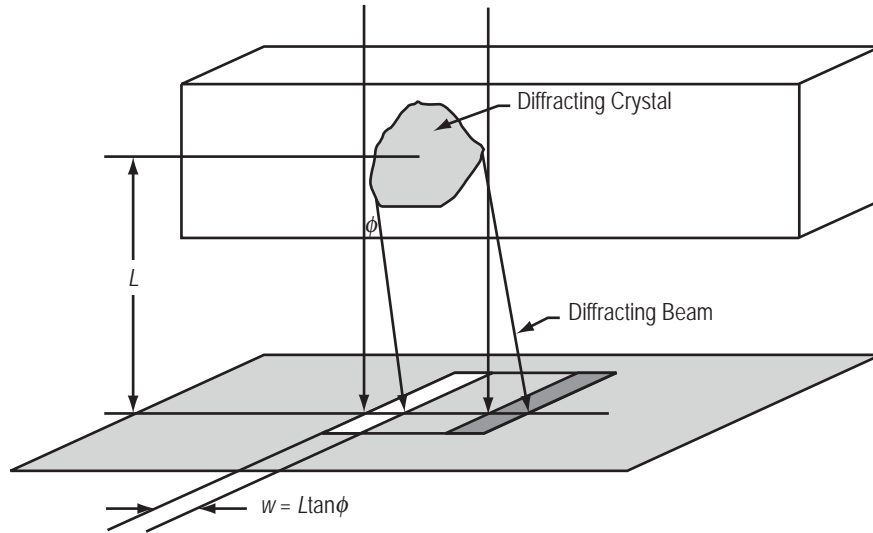$$\therefore \frac{1-\cos\phi}{\sin\phi} = \tan\theta$$

Figure 28. Formation of an image by a large diffracting crystal embedded in an amorphous medium. The shift in beam power by the diffracting component of the incident beam affects power intensity at the image boundaries.

If the effective distance from the diffracting body is L, then a portion of the beam passing through the body is deflected by approximately

$$w = 2L\frac{\tan\theta}{\left(1 - \tan^2\theta\right)} = L\tan 2\theta \ .$$

This displacement distance w is the width of lines on opposite sides of the displaced section image. On one side, the line is deprived of some radiation and is lighter; on the other side, the line receives extra radiation and is darker. This width changes as the beam is tilted by $\Delta\theta$. See table 5.

Table 5. Relationship of movement of a diffraction image with angular displacement of incident x-ray beam.

θ	w/L	θ	w/L
0°	0	25°	1.19
5°	0.18	30°	1.73
10°	0.36	35°	2.75
15°	0.58	40°	5.67
20°	0.84	45°	∞

Suppose there is a diffracting body in a 0.05-in-thick plate. If the center of the body is about three-fourths of the thickness toward the weld crown and the x-ray film is right on the bottom of the plate, then $L \approx 0.04$ in. If the initial observation happens to be with a beam angle θ of 20°, then the width of the line is 0.03 in.

Reducing the angle by 20° causes the lines to disappear. Increasing the angle by 20° causes the lines to widen to 0.21 in with a corresponding reduction in intensity.

Reducing the angle by 10° causes the line width to shrink to 0.01 in. Increasing the angle by 10° causes the line width to increase to 0.06 in.

The geometry of the diffracting body also affects the width of the enigma line. A discussion of this effect is not included here, but is left for a subsequent study.

REFERENCES

1. Quality Engineering Report No. 174, "Inconel Radiographic Images," PerkinElmer Fluid Sciences, Beltsville, MD, July 2003.

2. Muzyka, D.B.: "The Metallurgy of Nickel-Iron Alloys," Sims, C.T., and Hagel, W.C., *The Superalloys*, Chapter 4: Wiley Publications, NY, pp. 113–143, 1972.

3. Patel, S.J.; and Smith, G.D.: "Role of Niobium in Wrought Superalloys," *Niobium*, *Science & Technology: Proceedings of the International Symposium Niobium 2001*, December 2–5, 2001, The Minerals, Metals & Materials Society, pp. 1081–1108, 2002.

4. Morral F.R.: "Wrought Superalloys," *Metals Handbook*, *Vol. 3*, *Properties and Selection: Stainless Steels*, *Tool Materials and Special-Purpose Metals*, American Society for Metals, 9th Edition, pp. 207–241, 1980.

5. Yoshimura, H.; and Winterton, K.: "Solidification Mode of Weld Metal in Inconel 718," *The Welding Journal*, Vol. 52, p. 132–138, 1972.

6. Matlock, C.A.; Merrill, J.M.; Ambrose, B.C.; et al.: "Solidification Map of Directionally Solidified Inconel 718," Louthan, M.R., Jr. and Brooks, C.R., *Metallographic Characterization of Materials Behavior*, ASM International, pp. 51–60, 1994.

7. McIntire, P.; and Bryant, L.E.: *Nondestructive Testing Handbook*, *Vol. 3: Radiography and Radiation Testing*, *Edition 2*, American Society for Nondestructive Testing, pp. 384–417, 1985.

8. Cullity, B.D.: *Elements of X-Ray Diffraction*, Appendix 15, Addison-Wesley Publishing Company, Inc., Reading, MA, pp. 490–505, 1956.

REPORT DOCUMENTATION PAGE

Form Approved
OMB No. 0704-0188

1. AGENCY USE ONLY *(Leave Blank)*	2. REPORT DATE September 2007	3. REPORT TYPE AND DATES COVERED Technical Memorandum	
4. TITLE AND SUBTITLE Study of Radiographic Linear Indications and Subsequent Microstructural Features in Gas Tungsten Arc Welds of Inconel 718			**5. FUNDING NUMBERS**
6. AUTHORS J.L. Walley,* A.C. Nunes, J.L. Clounch,** and C.K. Russell			
7. PERFORMING ORGANIZATION NAME(S) AND ADDRESS(ES) George C. Marshall Space Flight Center Marshall Space Flight Center, AL 35812			**8. PERFORMING ORGANIZATION REPORT NUMBER** M–1201
9. SPONSORING/MONITORING AGENCY NAME(S) AND ADDRESS(ES) National Aeronautics and Space Administration Washington, DC 20546–0001			**10. SPONSORING/MONITORING AGENCY REPORT NUMBER** NASA/TM—2007–215075

11. SUPPLEMENTARY NOTES

Prepared by the Materials and Processes Laboratory, Engineering Directorate
*Universities Space Research Association, Huntsville, AL   **Jacob ESTS Group, Huntsville, AL

12a. DISTRIBUTION/AVAILABILITY STATEMENT Unclassified-Unlimited Subject Category 29 Availability: NASA CASI 301–621–0390	12b. DISTRIBUTION CODE

13. ABSTRACT *(Maximum 200 words)*

This study presents examples and considerations for differentiating linear radiographic indications produced by gas tungsten arc welds in a 0.05-in-thick sheet of Inconel 718. A series of welds with different structural features, including the enigma indications and other defect indications such as lack of fusion and penetration, were produced, radiographed, and examined metallographically. The enigma indications were produced by a large columnar grain running along the center of the weld nugget occurring when the weld speed was reduced sufficiently below nominal. Examples of respective indications, including the effect of changing the x-ray source location, are presented as an aid to differentiation. Enigma, nominal, and hot-weld specimens were tensile tested to demonstrate the harmlessness of the enigma indication. Statistical analysis showed that there is no difference between the strengths of these three weld conditions.

14. SUBJECT TERMS gas tungsten arc welding, Inconel 718, radiographic indications			15. NUMBER OF PAGES 44
			16. PRICE CODE
17. SECURITY CLASSIFICATION OF REPORT Unclassified	18. SECURITY CLASSIFICATION OF THIS PAGE Unclassified	19. SECURITY CLASSIFICATION OF ABSTRACT Unclassified	20. LIMITATION OF ABSTRACT Unlimited

National Aeronautics and
Space Administration
IS20
George C. Marshall Space Flight Center
Marshall Space Flight Center, Alabama
35812